Dynamic Routing for Flying Ad Hoc Networks

Stefano Rosati, *Member, IEEE*, Karol Krużelecki, *Member, IEEE*, Grégoire Heitz,
Dario Floreano, *Senior Member, IEEE*, and Bixio Rimoldi, *Fellow, IEEE*

***Abstract*—This paper reports experimental results on self-organizing wireless networks carried by small flying robots. Flying ad hoc networks (FANETs) composed of small unmanned aerial vehicles (UAVs) are flexible, inexpensive, and fast to deploy. This makes them a very attractive technology for many civilian and military applications. Due to the high mobility of the nodes, maintaining a communication link between the UAVs is a challenging task. The topology of these networks is more dynamic than that of typical mobile ad hoc networks (MANETs) and of typical vehicle ad hoc networks. As a consequence, the existing routing protocols designed for MANETs partly fail in tracking network topology changes. In this paper, we compare two different routing algorithms for ad hoc networks: optimized link-state routing (OLSR) and predictive OLSR (P-OLSR). The latter is an OLSR extension that we designed for FANETs; it takes advantage of the Global Positioning System (GPS) information available on board. To the best of our knowledge, P-OLSR is currently the only FANET-specific routing technique that has an available Linux implementation. We present results obtained by both media-access-control (MAC) layer emulations and real-world experiments. In the experiments, we used a testbed composed of two autonomous fixed-wing UAVs and a node on the ground. Our experiments evaluate the link performance and the communication range, as well as the routing performance. Our emulation and experimental results show that P-OLSR significantly outperforms OLSR in routing in the presence of frequent network topology changes.**

***Index Terms*—IEEE 802.11 Standard, routing protocols, unmanned aerial vehicles, vehicular ad hoc networks.**

I. Introduction

In the case of a calamitous event, when ordinary communication infrastructure is out of service or simply not available, a group of small flying robots can provide a rapidly deployable and self-managed ad hoc Wi-Fi network to connect and coordinate rescue teams on the ground. Networks of small unmanned aerial vehicles[1] (UAVs) can also be employed for wildfire monitoring [1], border surveillance [2], and for extending ad hoc networks on the ground [3]–[5].

The recent technological progress in electronics and communication systems, particularly due to the the widespread availability of low-cost micro-embedded computers and Wi-Fi radio interfaces, has paved the way for the creation of inexpensive flying ad hoc networks (FANETs); however, a challenging networking problem arises.

As pointed out in [6], FANETs are a special case of mobile ad hoc networks (MANETs) characterized by a high degree of mobility. In a FANET, the topology of the network can change more frequently than in a typical MANET or vehicle ad hoc network (VANET). As a consequence, the network routing becomes a crucial task [7], [8]. The network routing algorithms, which have been designed for MANETs, such as BABEL [9] or the optimized link-state routing (OLSR) protocol [10], [11], fail to follow the evolution of the network topology. It is possible to bypass this problem by considering star networks with static routing [12]. However, star architectures restrict the operative area of groups of UAVs, because the nodes cannot fly out of the communication range of the control center. In this paper, we focus on partially connected mesh ad hoc networks that enable the UAVs to use multihop communication to extend the operative area. In this case, the problem of highly dynamic routing must be faced.

A few methods for overcoming the problem caused by a rapidly changing network topology have recently been proposed: Guo *et al.* [13] present a UAV-aided cross-layer routing protocol that aims at improving the routing performance of a ground MANET network with aid from one UAV. In [14], Alshbatat and Dong propose the use of directional antennas and two cross-layer schemes called intelligent media access control (MAC) and directional OLSR. The latter is an extension of OLSR. The choice of the route is based on flight information (such as attitude variations, pitch, roll, and yaw). Only OPNET simulation results are reported. Benzaid *et al.* [15], [16] present an OLSR extension denoted fast OLSR that aims at meeting the need for highly dynamic routing in MANETs composed of *fast-moving* and *slow-moving* nodes. This extension increases the rate of the *Hello* messages only for the nodes that move faster than a given speed. If the *fast-moving* nodes are a small percentage of the network's nodes, the additional overhead is limited. Otherwise, if the network is composed mainly of UAVs, the overhead significantly grows. In [17], we present an extension to the OLSR protocol named predictive OLSR (P-OLSR). The key idea of this extension is to use Global Positioning System (GPS) information available on board and to weigh the expected transmission count (ETX) metric by a

Manuscript received May 6, 2014; revised February 23, 2015; accepted March 15, 2015. Date of publication March 26, 2015; date of current version March 10, 2016. This work was supported by armasuisse, competence sector Science+Technology for the Swiss Federal Department of Defense, Civil Protection, and Sport. The review of this paper was coordinated by Prof. J. Deng.

S. Rosati, K. Krużelecki, and B. Rimoldi are with the Mobile Communications Laboratory (LCM), Swiss Federal Institute of Technology (EPFL), 1015 Lausanne, Switzerland (e-mail: stefano.rosati@epfl.ch; karol.kruzelecki@epfl.ch; bixio.rimoldi@epfl.ch).

G. Heitz and D. Floreano are with the Laboratory of Intelligent Systems (LIS), Swiss Federal Institute of Technology (EPFL), 1015 Lausanne, Switzerland (e-mail: gregoire.heitz@epfl.ch; dario.floreano@epfl.ch).

Color versions of one or more of the figures in this paper are available online at http://ieeexplore.ieee.org.

Digital Object Identifier 10.1109/TVT.2015.2414819

[1]Small UAVs are also known as micro-air vehicles.

factor that takes into account the direction and the relative speed between the UAVs.

In this paper, we present field experiments that compare P-OLSR against OLSR. The experiments involved two UAVs and a ground station. The carriers were fixed-wing autonomous planes called *eBees* and developed by SenseFly [18]. Each plane carried an embedded computer-on-module and an 802.11n radio interface. The field-test results show that P-OLSR can follow rapid topology changes and provide a reliable multihop communication in situations where OLSR mostly fails. To assess the behavior of P-OLSR in larger networks, we carried out MAC-layer emulations considering a network composed of 19 UAVs. To the best of our knowledge, P-OLSR is currently the only FANET-specific routing technique that has an available Linux implementation. The open-source software of the P-OLSR daemon can be downloaded from [19].

The rest of this paper is organized as follows. In Section II, we highlight the differences between OLSR and P-OLSR. In Section III, we specify the modified structure of the *Hello* messages and describe the implementation of the P-OLSR daemon. In Section IV, we describe the testbed, and in Section V, we describe the experiments and present the results. In Section VI, we present the MAC-layer emulation we used to assess the P-OLSR performance in larger networks. Finally, we draw our conclusions in Section VII.

II. Routing for Flying Ad Hoc Networks

In [12], Frew and Brown analyze the networking for systems of small UAVs. They characterize four different network architectures: *direct-link*, *satellite*, *cellular*, and *ad hoc* (also called *mesh networking*). The *direct-link* and the *satellite* architecture are star networks where all the UAVs are either directly connected to the ground control or to a satellite connected to the ground control. This is a simple network architecture: It does not require dynamic routing, because all the nodes are directly connected with the control center. The nodes require, however, long-range (terrestrial or satellite) links; hence, they are not suitable for small UAVs. Furthermore, UAV-to-UAV communication is inefficiently routed through the control center, even if the nodes operate the same area. This might cause traffic congestion in the control center, which is also a weakness of the system in case of attack.

In the *cellular* architecture, the UAVs are connected to a cellular system with many base stations scattered on the ground. UAVs can do a handover between different base stations during the flight. This architecture does not need a single vulnerable control center. However, the operating area of the UAVs is limited by the cellular network extension. In the case of a catastrophic event, the UAV system can be deployed only if the cellular network is present and functioning in the area.

In the *ad hoc* architecture, every node can act as a router. These networks are also known as FANETs: They have no central infrastructure; therefore, they are very robust against isolated attacks or node failures. Moreover, as these networks do not rely on any external support, they can be rapidly deployed anywhere. These characteristics, on one hand, make FANETs the most suitable solution for many applications, but on the other hand, they raise a challenging networking problem.

In fact, due to the rapid and erratic movement of the UAVs, the topology of a FANET can vary rapidly and the nodes must react by automatically updating their routing tables. Therefore, in a FANET, it is crucial to employ a fast and reactive routing procedure. In [17], we show that some of the most popular routing algorithms for MANETs, such as OLSR and BABEL, fail to track the fast topology changes of a FANET. Similar conclusions are also drawn in [7]. For this reason, in [17], we introduce P-OLSR. To predict how the quality of the wireless links between the nodes is likely to evolve, P-OLSR exploits the GPS information, which is typically available from the UAV's autopilot. For the sake of completeness, here, we briefly report the definition of ETX, as well as the key concepts behind P-OLSR.

A. Link-Quality Estimation

OLSR is currently one of the most popular proactive routing algorithms for ad hoc networks. It is based on the link-state routing protocol. The original OLSR design does not consider the quality of the wireless link. The route selection is based on the hop count metric, which is inadequate for mobile wireless networks. However, by using the ETX metric [20], the OLSR *link-quality* extension enables us to take into account the quality of the wireless links. The ETX metric was introduced in [21], and it is defined as

$$\mathrm{ETX}(\mathcal{R}) = \sum_{\eta\in\mathcal{R}} \mathrm{ETX}(\eta) = \sum_{\eta\in\mathcal{R}} \frac{1}{\phi(\eta)\rho(\eta)} \tag{1}$$

where $\mathcal{R}$ is a route between two nodes of the network, and η is a hop of the route $\mathcal{R}$. $\phi(\eta)$ is the forward receiving ratio, i.e., the probability that a packet sent through the hop η is successfully received. $\rho(\eta)$ is the reverse receiving ratio, i.e., the probability that the corresponding ACK packet is successfully received. In other words, ETX estimates the expected number of transmissions (including retransmissions) necessary to deliver a packet from the source to its final destination. Then OLSR selects the route that has the smallest ETX, which is not necessarily that with the least number of hops. If all the hops forming $\mathcal{R}$ are errorless (i.e., $\phi(\eta) = \rho(\eta) = 1$), $\mathrm{ETX}(\mathcal{R})$ is equal to the number of hops of $\mathcal{R}$.

The receiving ratios are typically estimated by link-probe messages. The OLSR link-quality extension uses the control messages named *Hello* messages as a link probe. ϕ is computed by means of an exponential moving average, as follows:

$$\begin{cases} \phi_l = \alpha h_l + (1-\alpha)\phi_{l-1} \\ \phi_0 = 0 \end{cases}, \quad 0 \le \alpha \le 1 \tag{2}$$

where

$$h_l = \begin{cases} 1 & \text{if the } l\text{th } Hello \text{ message is received} \\ 0 & \text{otherwise} \end{cases} \tag{3}$$

and α is an OLSR parameter, named *link-quality aging*, that drives the tradeoff between the accuracy and responsiveness of the receiving ratio estimation. On one hand, with a greater α, the receiving ratios will be averaged for a longer time, thus yielding a more stable and reliable estimation. On the other hand, with a lower α, the system will react faster. Another important OLSR parameter is the *Hello interval* (HI) that indicates how frequently *Hello* messages are broadcasted.

B. *Speed-Weighted ETX*

In a FANET, the nodes move rapidly; for example, the cruising speed of our flying robots is around 12 m/s. The network topology changes rapidly, and a wireless link between two UAVs can break suddenly. In these networks, the ETX metric might be inadequate, because it is not reactive enough to follow the link variations. Due to the delay introduced by the exponential moving average, a node notices that a certain wireless link has broken with a nonnegligible delay. Therefore, for a significant amount of time, it will continue routing packets on a link that is actually broken.

To solve this problem, we modify the ETX metric to take into account the position and the direction of the UAV, with respect to its neighbors. The ETX(η) metric of the hop η between the nodes i and j is weighed by a factor that accounts for the relative speed between i and j as follows:

$$\mathrm{ETX}(\eta) = \frac{e^{v_\ell^{i,j}\beta}}{\phi(\eta)\rho(\eta)} \tag{4}$$

where $v_\ell^{i,j}$ is the relative speed between nodes i and j, and β is a nonnegative parameter.

If the nodes i and j move closer to each other, the relative speed is negative; thus, the ETX will be weighted by a factor smaller than 1. Otherwise, if the nodes i and j move apart from each other, the relative speed is positive; thus, the ETX will be weighted by a factor greater than 1. In other words, a hop between two nodes that move closer to each other is preferred rather than a hop between two nodes that move apart, even if they have the same values of ϕ and ρ.

To compute the speed-weighted ETX, we assume that every node knows the position of its neighbors. As illustrated in Appendix III, to distribute the GPS coordinates across the network, we add a field to the *Hello* messages.

The instantaneous relative velocity between i and j at time t_i is computed as

$$\tilde{v}_\ell^{i,j} = \frac{d_\ell^{i,j} - d_{\ell-1}^{i,j}}{t_\ell - t_{\ell-1}} \tag{5}$$

where t_ℓ and $t_{\ell-1}$ are the arrival time of the last and second to last *Hello* message. $d_\ell^{i,j}$ and $d_{\ell-1}^{i,j}$ are the corresponding distances between nodes i and j. As the GPS positions are subject to errors and gusts of wind can perturb the motion of the UAVs, it is preferable to average the instantaneous speed using a exponential moving average as follows:

$$\begin{cases} v_\ell^{i,j} = \gamma \tilde{v}_\ell^{i,j} + (1-\gamma) v_{\ell-1}^{i,j} \\ v_0^{i,j} = 0 \end{cases}, \quad 0 \le \gamma \le 1 \tag{6}$$

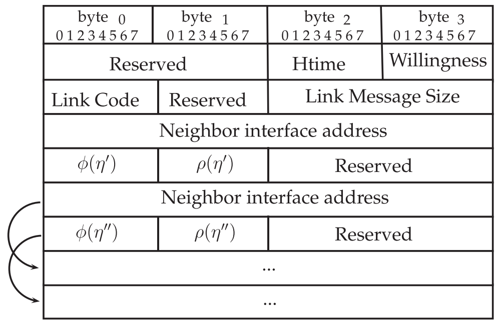

byte 0 01234567	byte 1 01234567	byte 2 01234567	byte 3 01234567
Reserved		Htime	Willingness
Link Code	Reserved	Link Message Size	
Neighbor interface address			
$\phi(\eta')$	$\rho(\eta')$	Reserved	
Neighbor interface address			
$\phi(\eta'')$	$\rho(\eta'')$	Reserved	
...			
...			

Fig. 1. Format of the original (i.e., OLSRd) *Hello* message.

where γ is a P-OLSR parameter. Acting on the P-OLSR parameter β and γ, we can optimize the routing selection to the cruising speed of the UAVs and to the chosen HI.

Fixed-wing UAVs require forward motion for flying. They also require a minimum air-speed and turning radius. Therefore, the direction of the UAV is a good indicator for predicting its position in the near future and to foresee how the link quality is likely to evolve.

III. Implementation Details

To implement the P-OLSR protocol, we forked an open-source implementation of OLSR called OLSRd [22]. In the modified version, the *Hello* messages are augmented to contain position information. Thus, every node knows its neighbors' positions and can compute the corresponding ETX according to (4).

A. *OLSRd With Link-Quality Extension*

OLSRd uses link-quality sensing and ETX metrics through the so-called *link-quality* extension [20]. It replaces the hysteresis mechanism of the OLSR protocol with link-quality sensing algorithms that are intended to be used with ETX-based metrics. To do so, the *link-quality* extension uses the OLSR *Hello* messages to probe link quality and to advertise link-specific quality information, (i.e., receiving ratios, ϕ and ρ), in addition to detecting and advertising neighbors. Likewise, it includes the link-quality information also in OLSR topology control (TC) messages that are to be distributed to the whole network. Clearly, the modified messages are no longer RFC compliant because they include new fields for link-quality information. Therefore, all the nodes in the network have to use the link-quality extension.

B. *P-OLSRd Implementation*

To implement P-OLSR, we have to share the coordinates (i.e., longitude, latitude, and altitude) of each node with its neighbors. This is done through the *Hello* messages. Subsequently, each node uses its neighbors' coordinates to compute the corresponding relative speeds and shares them across the whole network via both *Hello* and TC messages.

Fig. 1 shows the structure of the original *Hello* message in OLSRd. The first block of 8 bytes carries information about the

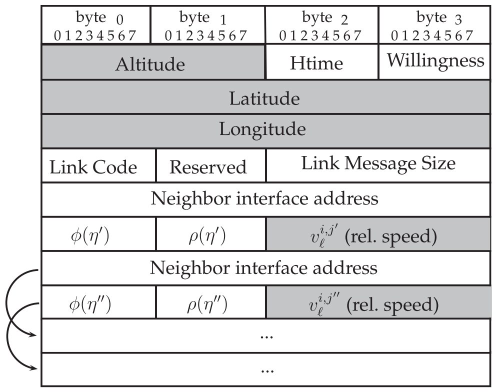

Fig. 2. Format of the modified (i.e., P-OLSRd) *Hello* message.

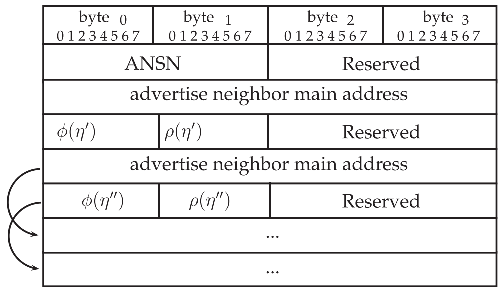

Fig. 3. Format of the original (i.e., OLSRd) *topology control* message. ANSN stands for advertised neighbor sequence number.

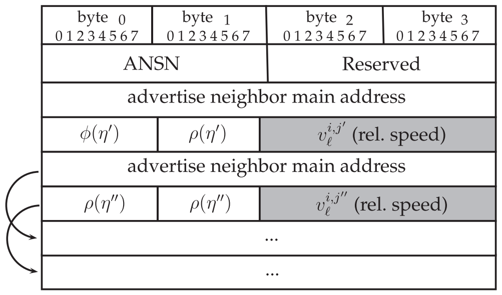

Fig. 4. Format of the modified (i.e., P-OLSRd) *topology control* message.

node itself. Note that, in this block, there are 3 reserved bytes that are not used by the OLSR daemon and are filled with zeros. Then, a block of 8 bytes is appended for each neighbor seen by the node. This block is formatted as follows: 4 bytes are for the IP address of the neighbor, 1 byte is for the forward receiving ratio[2] $\phi(\eta')$, 1 byte is for the reverse receiving ratio $\rho(\eta')$, and 2 bytes are not used, and hence, they filled with zeros.

Fig. 2 shows the modified structure of the *Hello* message. We highlight in gray the fields that were added or modified. The first part of the message contains 16 bytes instead of 8. It contains the latitude and the longitude, formatted as single-precision floating-point numbers that occupy 4 bytes each.[3] The altitude is formatted as a 16-bit fixed-point number that replaces the 2 reserved bytes not used by the OLSR daemon. Similarly to the original *Hello* message, a block of 8 bytes is appended for each neighbor seen by the node. The only difference here is that we use the 2 empty bytes to communicate the averaged relative speed between the nodes. The speed is formatted as a 16-bit fixed-point number.

The size difference between the original and the modified *Hello* message is 8 bytes, independently of the numbers of nodes in the network. The *Hello* message is encapsulated into a UDP datagram that, in turn, is encapsulated in an IP packet and then into an 802.11 frame. For medium and large networks, the additional 8 bytes constitute a negligible overload compared with the total size of the frame.

Figs. 3 and 4 show the structure of the TC message for OLSRd and P-OLSRd, respectively. They differ only by one field: P-OLSRd exploits the 2 reserved bytes to convey the averaged relative speed formatted as a 16-bit fixed-point number. The original and the modified TC message have the same size.

IV. UAV Testbed

We can distinguish two main types of small UAVs: rotary-blade and fixed-wing. Rotary-blade UAVs, which are also known as minicopters or multicopters, fly using the lift force generated by one or more blades, such as helicopters. Typically, rotary-blade UAVs are composed of four blades; in this case, they are known as quadricopters. They are able to take off and land vertically, fly in every direction, and maintain a fixed position in the air.

Fixed-wing UAVs fly by exploiting the lift force generated by the forward speed of the vehicle in the air; hence, forward motion is required for flying. They have a minimum speed and turning radius and can fly at higher speeds and with a higher energy efficiency compared with rotary-blade UAVs. Therefore, they can cover a greater area, but the network topology is likely to change very rapidly. This makes the ad hoc networking of fixed-wing UAVs more challenging and, at the same time, more interesting.

In this paper, we address fixed-wing UAVs instead of those with rotary blades. For the experiments, we use two fixed-wing UAVs, named *eBee*, developed by SenseFly [18]. The vehicle's body is made of expanded polypropylene, and it has a single rear-mounted propeller powered by an electric motor. The *eBee* platform is shown in Fig. 5(a). It has an integrated autopilot capable of flying with winds up to 12 m/s, at a cruising speed of about 57 km/h, with an autonomy of 45 min. In case of emergency, they can be remotely controlled up to a distance of 3 km via a Microhard Systems Nano n2420 [23] link connection, and this low-data-rate control link is only used for controlling the plane. The data produced by the UAV are instead carried by the 802.11n link. Due to its small dimensions (the wing span is 96 cm) and weight (under 630 g), flying *eBees* are not considered to be dangerous. In some countries (e.g., Switzerland), they can be used without specific authorization.

On each plane, we mount a Gumstix Overo Tide [24], which is an ARM-based computer-on-module produced by Gumstix

[2] η' is the hop between the node that is producing the *Hello* message and its neighbor.

[3] To have at least 1-m precision, we could have formatted the latitude and longitude with 26-bit fixed-point representation each. This, however, would have required rearranging the latitude and longitude and adding some padding to complete the byte.

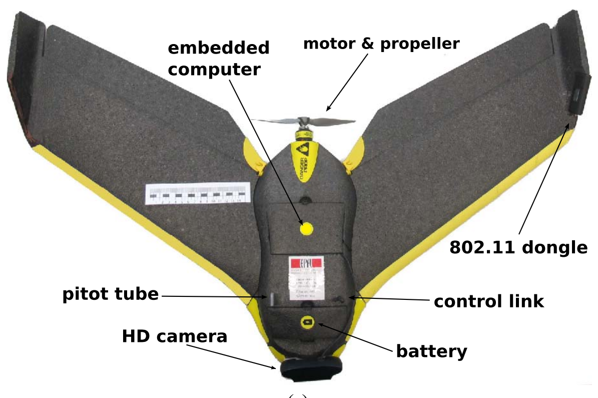

(a)

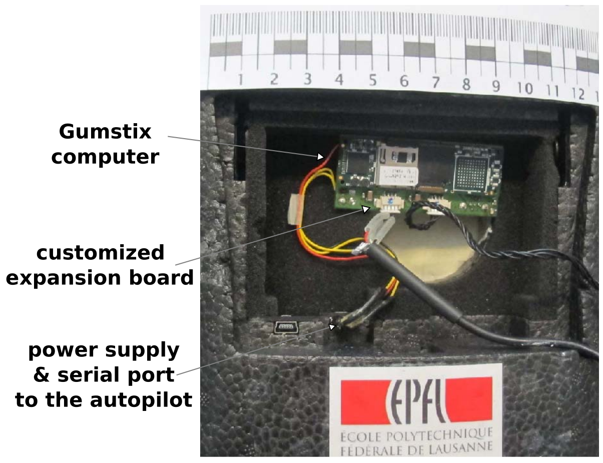
Gumstix computer
customized expansion board
power supply & serial port to the autopilot

(b)

Fig. 5. UAV platform used in the experiments. (a) SenseFly *eBee* with HD camera, Linksys AE3000 USB dongle, and Gumstix computer-on-module. (b) Computer and expansion board in the rear compartment of the UAV.

Inc. The computer runs a customized Linux distribution (kernel version 3.5.0), and it is connected to a compatible expansion board that we designed and produced. The expansion board incorporates a USB 2.0 hub with four powered ports and a serial port connected to the autopilot. Using this serial port, the Gumstix can fetch the current GPS data, as well as other flight parameters. The computer is also connected via USB to an HD camera and to a Wi-Fi radio interface. The embedded computer setup is shown in Fig. 5(b).

The Wi-Fi radio interface is the Linksys AE3000 USB dongle, using 802.11n. Despite the small dimensions, they support a MIMO system with three antennas. During the experiments, we enabled 802.11n space–time block coding to exploit channel diversity. The transmission bandwidth was set to 20 MHz in the 5-GHz unlicensed band. We used quaternary phase-shift keying modulation, code rate 1/2, and one spatial stream (MODCOD 1).

V. Experiments

Here, we describe the two experiments that we carried out on the EPFL campus. The aim of the first experiment was to characterize the end-to-end link performance between an UAV and a node on the ground. Specifically, we determined the communication range in which the two nodes can communicate with a tolerable amount of lost packets. In the second experiment, we compared the OLSR protocol with the P-OLSR protocol.

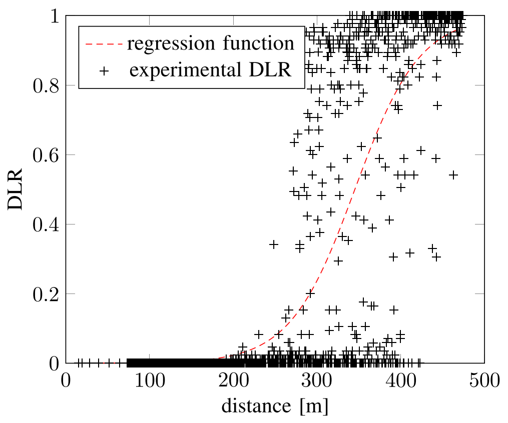

Fig. 6. Experimental DLR versus distance. The black crosses are the DLR measured values, and the dashed red line is the corresponding nonlinear least squares regression function.

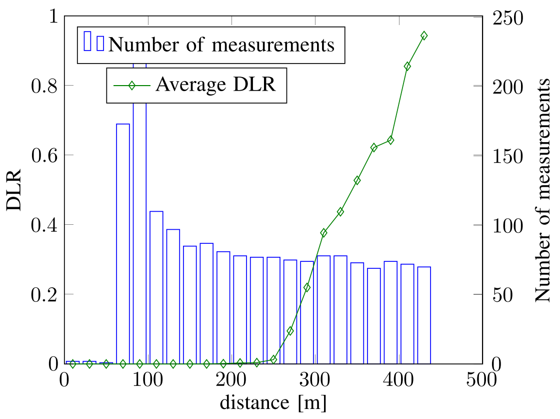

Fig. 7. Average DLR versus distance. The blue bars represent the number of measurements per distance interval. The green solid line is the average DLR.

A. *Link Performance Assessment*

In this experiment, we had a two-node network composed of a node on the ground and a flying UAV. The UAV flew between two checkpoints positioned 450 m apart. For both checkpoints, we set a turning radius of 30 m, and the height-above-ground was 75 m. The node on the ground was located at the center of one of the checkpoints. Using *iperf*, we took one measurement of the link quality per second. Every second, the UAV sent 85 UDP datagrams (totaling 1 Mb) to the node on the ground. All the datagrams received with a delay greater than 5 s were considered lost. We also counted as correctly received the datagrams that arrived out of order (provided that their delay was smaller than 5 s). This is what can be tolerated by a video streaming, where the video is played with a 5-s delay. Every second, we computed the datagram loss rate (DLR), which is the ratio between the datagram lost and their total number.

The results are reported in Fig. 6. The black crosses represent the DLR measured at a given distance. The dashed line

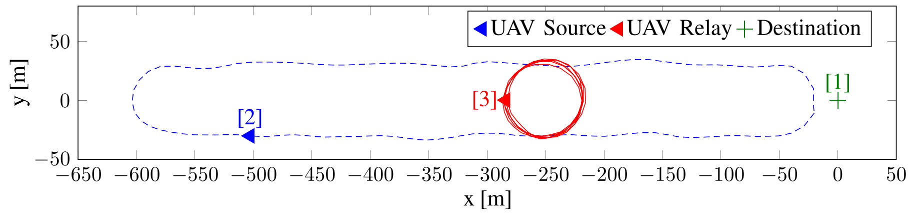

Fig. 8. Trajectories of the UAVs during the network field experiments.

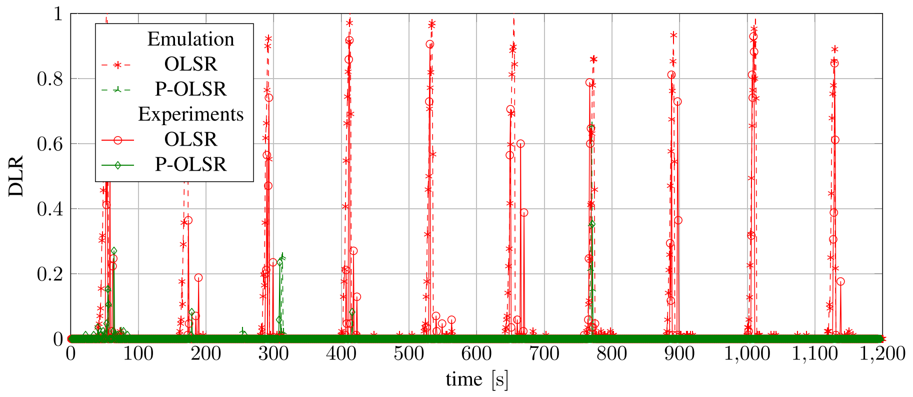

Fig. 9. Evolution of the average DLR. Dashed lines report the results of MAC-layer emulations, and solid lines report the results of field experiments.

represents the corresponding nonlinear least squares regression function. The function that we use as a model is

$$\frac{1}{1+e^{-(p_1+p_2 d)}} \tag{7}$$

where d is the distance in meters, and p_1 and p_2 are the coefficients to be estimated. Using a nonlinear fitting method, we compute the value of p_1 and p_2, thus yielding the best fitting in the least squares sense. They are $p_1 = 8.9$ and $p_2 = 0.025$.

In Fig. 7, we quantize the distance between the transmitter and the receiver with a bin width of 20 m. For each bin, we compute the average DLR. The resulting curve is plotted in green. We also report the number of measurements per bin.

As we can see from these results, the connection is good when the distance is shorter than 250 m. In this region, the observed DLR is always lower than 0.2. We observe a transition from 250 m to 300, where the DLR can be as high as 1, but on average, it is lower than 0.3. When the distance is greater than 300 m, the connection significantly degrades, and the DLR is often close to 1. The average DLR is 0.5 at 350 m. We observe some sporadic cases of a good connection, even when the distance is greater than 400 m.

B. Routing Performance Assessment

In the second experiment, we compared the routing performance of OLSR with link-quality extension and P-OLSR. For both OLSR and P-OLSR, we set the HI equal to 0.5 s. This value is a good tradeoff between the amount of overhead and the reactivity speed of the algorithm. Using the default HI value, which, in OLSRd, is equal to 2 s, the algorithm would have been too slow to pursue the topology changes. As P-OLSR exploits the GPS information to estimate the link-quality evolution, it could also work with a longer HI. Nevertheless, for the sake of fairness, we use the same value for both algorithms.

We set the *link-quality aging*, α, equal to 0.2 for OLSR and to 0.05 for P-OLSR. This parameter controls the tradeoff between the accuracy and the responsiveness of the receiving ratio estimation. As before, as P-OLSR can predict the link-quality evolution, it can work with a smaller α, yielding a more accurate estimation of the receiving ratio. OLSR, on the contrary, needs a greater aging value to increase its responsiveness, at the expense of accuracy. The other P-OLSR parameters were $\beta = 0.2$ and $\gamma = 0.04$.

We had a network of three nodes: one fixed destination on the ground (Node 1), one flying UAV source (Node 2), and one flying UAV relay (Node 3). Node 1 was on the terrace of the BC building on the EPFL campus (latitude: 46.51843° N; longitude: 6.561591° E). The UAV source Node 2 flew following a straight trajectory of 600 m west from Node 1, and then it returned to the starting point. The UAV relay Node 3 followed a circular trajectory of radius 30 m and centered at 250 m west from Node 1. Both the UAVs flew about 75 m above the ground, and the terrace of the BC building is approximately 10 m above the ground. The actual trajectories followed by the planes are shown in Fig. 8.

We performed ten loops for each routing algorithms. The loop time is affected by the weather conditions, particularly the wind. During our experiment, the eBee took, on average, 120 s to complete a loop. The time difference between the fastest and the slowest loop was around 10 s. In each loop, Node 2 changed its routing to reach Node 1, from a direct connection to a two-hop connection, and *vice versa*. Therefore, the network topology was expected to change two times during the each loop.

Fig. 9 shows the evolution of the DLR during the ten runs. For OLSR, we notice some peaks of the DLR that correspond

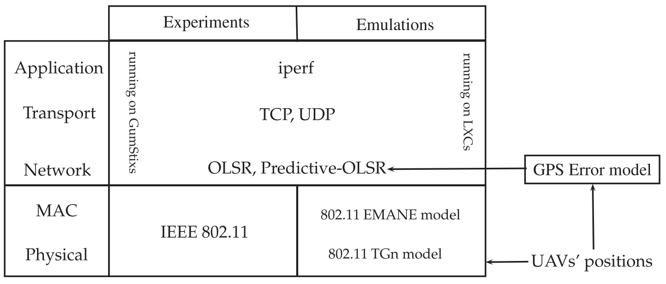

Fig. 10. Emulation platform.

to the moments when the routing algorithm has to switch from the direct link to a two-hop. This happens because OLSR takes several seconds to detect that a wireless direct link is broken. This translates into an interruption of the service. P-OLSR, however, reacts promptly to topology changes. As we can see from the field-test results, P-OLSR is able to predict a change in the topology and reacts before the previous link breaks. The DLR peaks that we see on the P-OLSR results are due to the fading of the wireless channels rather than to incorrect routing.

VI. Media Access Control-Layer Emulations With Larger Networks

Here, we examine the behavior of P-OLSR operating on larger FANETs. When many UAVs are involved, field experiments become expensive. For this reason, we analyze the performance of P-OLSR via a network emulation platform that integrates all the testbed aspects.

A. Emulation Platform

To analyze the routing performance in medium/large FANETs, we developed the emulation platform shown in Fig. 10. It creates a Linux container (LXC) for each node of the network. The nodes are connected using a MAC-layer real-time emulator called an extendable mobile ad hoc network emulator (EMANE). EMANE is an open-source framework, developed primarily by the Naval Research Laboratory [25]. The MAC and the physical layers are emulated, whereas the remaining layers use the real software implementations used by the Linux machine. For a propagation channel model, we use the IEEE 802.11 TGn model D, which is defined in [26]. This model was proposed for outdoor environments with line-of-sight conditions. EMANE imports the positions of the UAVs from log files and uses them to compute the path loss for each link. These log files can be obtained from real-flight data logs or by a flight simulator that reproduces realistic flight conditions. Before passing the UAV's position to the P-OLSR daemon, we add an error to take into account imperfect GPS receivers. We model GPS errors following the statistical characterization of GPS error provided in [27].

B. Emulation Results

We carried out two network emulation campaigns. In the first campaign, we reproduced the conditions we had in the experiments. This was done to test the emulator. We used the positions reported in the log files of the actual experiments.

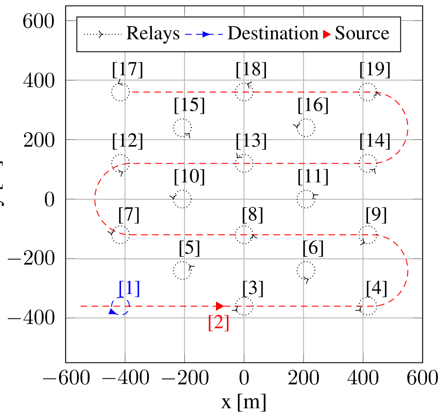

Fig. 11. Emulation setup. A network composed of 19 nodes. Node 2 is flying with a speed of 12 m/s following the trajectory markers with a red dashed line.

Fig. 9 shows emulation results (dashed lines) side-by-side with the experimental results (solid lines) for OLSR and for P-OLSR. The emulation results match with the experimental results.

In the second emulation campaign, we assessed the behavior of P-OLSR in larger networks, and we analyzed the role of various parameters, namely, the *HI*, the link-quality aging (α), and the P-OLSR-specific parameters (β and γ). The network consisted of 19 moving UAVs. One UAV (Node 2) scanned a rectangular area of 1200 m^2, by following the trajectory plotted with a dashed line in Fig. 11. It took 380 s to complete the trajectory. The other UAVs (Nodes $1, 3, \ldots, 19$) are uniformly spread within the area. They circulated around the respective waypoints, reproducing the behavior of actual fixed-wing UAVs. The radius of the circular trajectories was 30 m, the speed was 12 m/s, and the initial phase was uniformly distributed between zero and 2π. The distance between the relays was such that only the closest neighbors had a direct link. For example, Node 10 can communicate directly only with Nodes 5, 7, 8, 12, 13, and 15.

As we did in the experiments, we sent 85 UDP datagrams per second (totaling 1 Mb) from Node 2 to Node 1 using *iperf*. To have a more compact representation of the results, we compared the network performance in terms of average outage time. We say that an outage occurs when the DLR becomes greater than 0.2. The outage duration of such an event is the length of the interval during which the DLR stays above 0.2. The outage time of a run is the sum of all the outage durations. To average the results, we repeated the emulation ten times for each configuration.

In Figs. 12 and 13, we compare OLSR and P-OLSR for different durations of the HI while keeping the aging parameter α equal to 0.2. We present several P-OLSR configurations: In Fig. 12, we maintain a fixed value of β, ($\beta = 0.2$), and we vary the speed aging parameter γ. In Fig. 13, we fix γ ($\gamma = 0.08$), and we vary the value of β. Notice that P-OLSR drastically reduces the outage time compared with OLSR. In all its configurations, P-OLSR cuts down the outage time by at least 85%. Considering only the best performing P-OLSR configurations, the outage reduction is about 95%, 92%, and 90%, for HI durations equal to 0.5, 1, and 2 s, respectively.

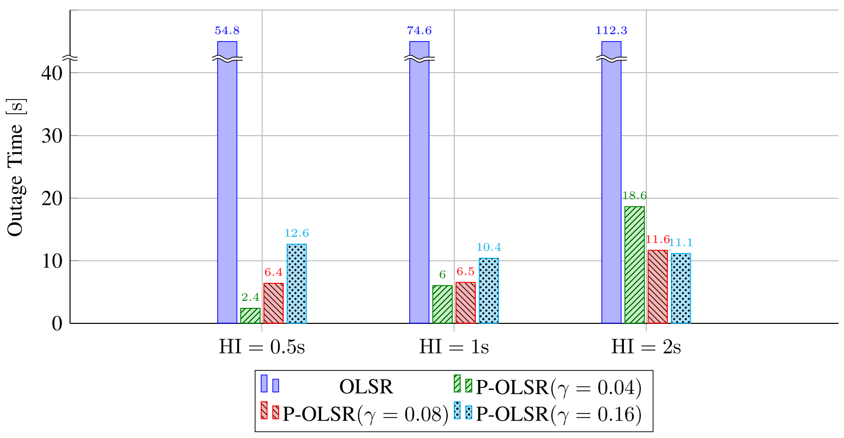

Fig. 12. Average outage time for OLSR and P-OLSR with $\alpha = 0.2$, $\beta = 0.2$, and different HI values.

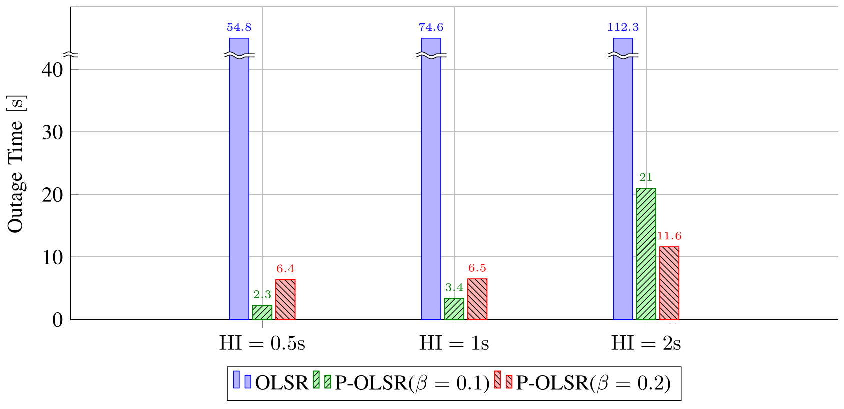

Fig. 13. Average outage time for OLSR and P-OLSR with $\alpha = 0.2$, $\gamma = 0.08$, and different HI values.

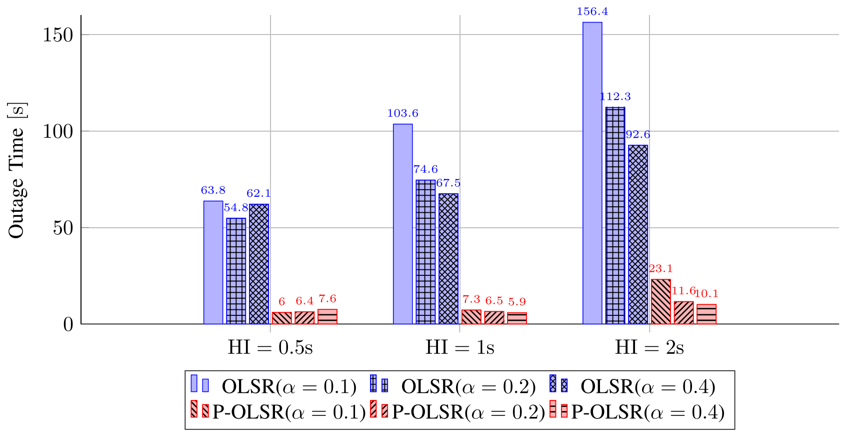

Fig. 14. Average outage time for OLSR and P-OLSR with different HI values and α.

In Fig. 12, we compare P-OLSR configurations for different values of γ. We see that when the HI is short, it is convenient to decrease the value of γ, and *vice versa*, because if the *Hello* message rate is low, it is convenient to have a fast aging of the previous speed estimates. In Fig. 13, we examine the role of the parameter β. We notice that when the HI is long, it is more convenient to increase β, which means that the speed term has a greater weight in the EXT computation [see (4)]. Intuitively, when the *Hello* message rate is low, the link-quality estimation is slow in tracking the channel fluctuations; therefore, it is convenient to give more weight to the speed term than to the link-quality term.

In Fig. 14, we can examine the role of the HI and the link-quality aging, i.e., α. We compare P-OLSR and OLSR considering different values of aging and different HI durations. To avoid overcrowding the plots, we consider only one P-OLSR configuration, that is, $\beta = 0.2$ and $\gamma = 0.08$.

As we notice in Fig. 14, the shorter the HI, the better the performance. However, the improvement brought by halving the HI from 1 to 0.5 s might not be large enough to justify

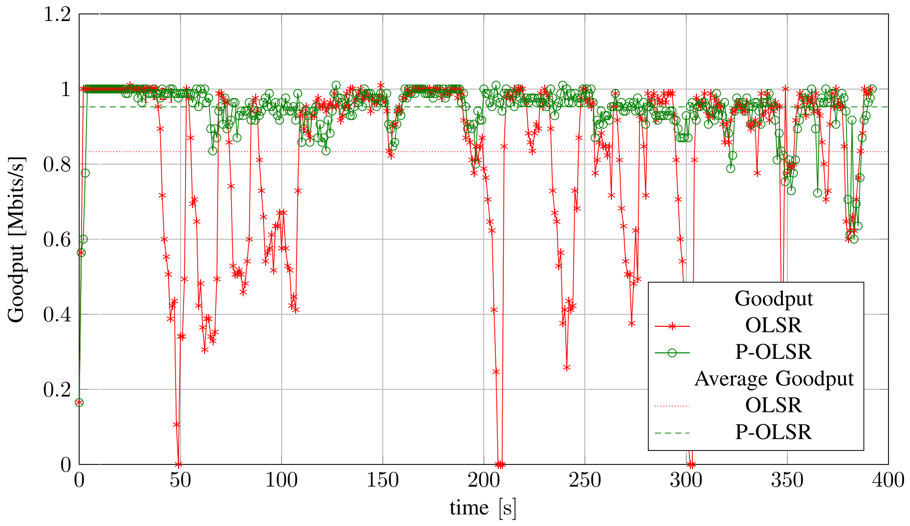

Fig. 15. Goodput during an emulation, considering HI $= 1$ s, $\alpha = 0.1$, $\beta = 0.2$, and $\gamma = 0.08$.

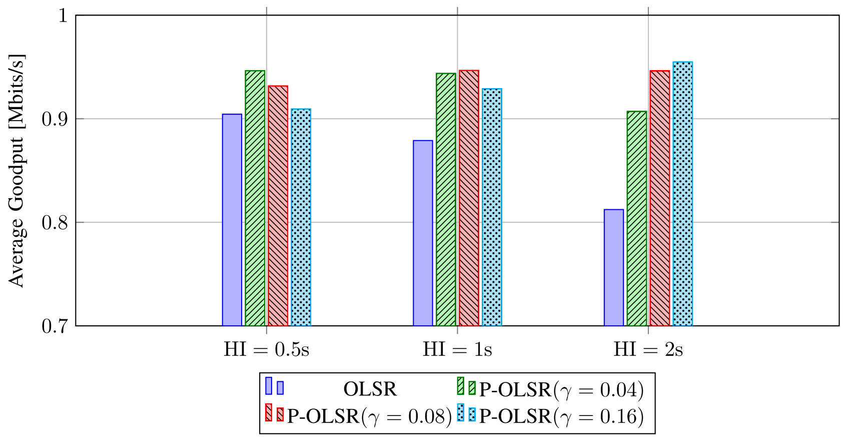

Fig. 16. Average goodput for OLSR and P-OLSR with $\alpha = 0.2$, $\beta = 0.2$, and different HI values.

the increase of the signaling traffic. This is more evident when P-OLSR is used. In fact, by exploiting the GPS information, P-OLSR is able to track the evolution of the network topology also when the *Hello* message rate is lower. As an example, we note that P-OLSR with HI of 2 s reduces the outage time by 80% with respect to OLSR with HI $= 0.5$ s, even if it generates about one fourth of the *Hello* messages.

We also compare the performance in terms of goodput. In perfect link conditions, the goodput is equal to 1 Mb/s. In Fig. 15, we plot the goodput achieved by OLSR and P-OLSR during an emulation with HI $= 1$ s, $\alpha = 0.1$, and the P-OLSR-specific parameters $\gamma = 0.08$ and $\beta = 0.2$. As can be seen from the plot, the goodput achieved by OLSR is unstable. It often drops below 0.6 Mb/s, and it also reaches zero. This is because OLSR does not promptly react to the topology changes. On the other hand, P-OLSR, which promptly reacts to topology changes and avoids outages, achieves a more stable goodput. It never drops under 0.6 Mb/s, and most of the time, it is above 0.8 Mb/s. The goodput is lower than 1 Mb/s because some packets are lost due to random channel fluctuations. In the plot, we report also the average goodput over the whole emulation duration, which is 0.83 Mb/s for OLSR and 0.95 Mb/s for P-OLSR. All the other cases behave similarly. For the sake of more compact representations, for the other cases, we report the average goodput over the emulation duration (see Figs. 16–18). As before, we repeated the emulation ten times for each configuration and report the average results. In Figs. 16 and 17, we compare OLSR and P-OLSR for several HI values while keeping $\alpha = 0.2$. In Fig. 16, we fix the value of β, ($\beta = 0.2$) and vary γ. In Fig. 17, we fix the value of γ ($\gamma = 0.08$) and vary β. We see that in all cases, P-OLSR increases the average goodput compared with OLSR. The gap is greater when the *Hello* message rate is lower (HI $= 2$ s), because OSLR is slower to react to topology changes. In Fig. 18, we compare P-OLSR and OLSR considering different values of aging and different HI durations. Again, to avoid overcrowding the plots, we consider only the P-OLSR configuration with $\beta = 0.2$ and $\gamma = 0.08$. Once again, P-OLSR outperforms OLSR in every configuration. The gap is smaller when the *Hello* message rate is high.

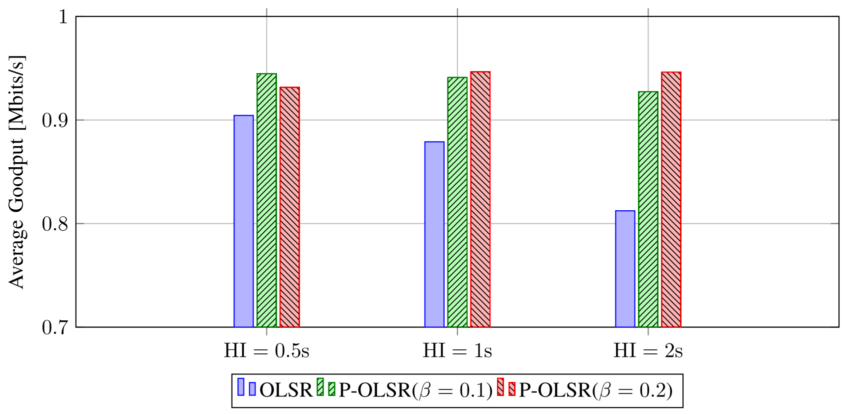

Fig. 17. Average goodput for OLSR and P-OLSR with $\alpha = 0.2$, $\gamma = 0.08$, and different HI values.

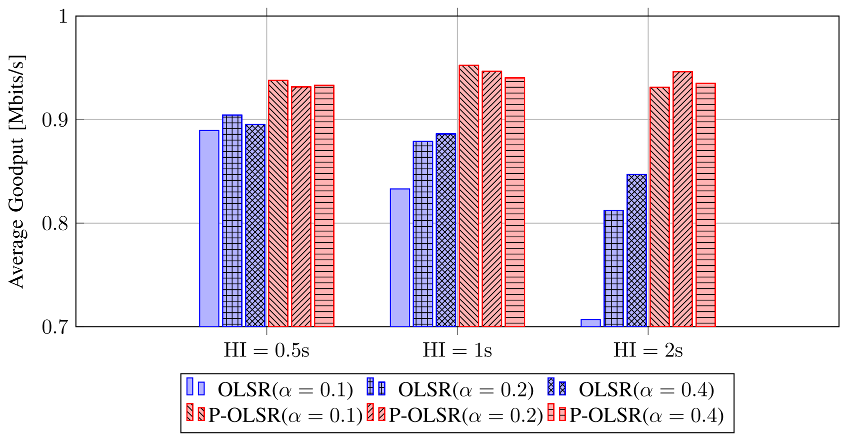

Fig. 18. Average goodput for OLSR and P-OLSR with different HI values and α.

VII. Conclusion

In this paper, we have compared the performance of P-OLSR and that of OLSR in a FANET composed of small fixed-wing UAVs.

Such networks are characterized by a high degree of mobility, which constitutes a challenge to the routing protocol. Routing protocols designed for MANETs mostly fail in tracking the evolution of the network topology. We address this problem by designing an OLSR extension, called P-OLSR: It takes advantage of the GPS information to predict how the quality of the wireless links will evolve. The network emulations and field experiments confirm our expectations. With P-OLSR, the routing follows the topology changes without interruptions, which is not the case with OLSR. We make use of P-OLSR to improve the routing in the SMAVNET II project [19]. SMAVNET II is a research project for developing a self-organizing UAV network.

References

[1] C. Barrado *et al.*, “Wildfire monitoring using a mixed air–ground mobile network,” *IEEE Pervasive Comput.*, vol. 9, no. 4, pp. 24–32, Oct. 2010.

[2] Z. Sun *et al.*, “BorderSense: Border patrol through advanced wireless sensor networks” *Ad Hoc Netw.*, vol. 9, no. 3, pp. 468–477, May 2011. [Online]. Available: http://dx.doi.org/10.1016/j.adhoc.2010.09.008

[3] I. Rubin and R. Zhang, “Placement of UAVs as communication relays aiding mobile ad hoc wireless networks,” in *Proc. IEEE MILCOM*, Oct. 2007, pp. 1–7.

[4] E. P. de Freitas *et al.*, “UAV relay network to support WSN connectivity,” in *Proc. IEEE ICUMT*, 2010, pp. 309–314. [Online]. Available: http://dx.doi.org/10.1109/ICUMT.2010.5676621

[5] F. Jiang and A. Swindlehurst, “Dynamic UAV relay positioning for the ground-to-air uplink,” in *Proc. IEEE GC Wkshps*, Dec. 2010, pp. 1766–1770.

[6] I. Bekmezci, O. K. Sahingoz, and S. Temel, “Flying ad-hoc networks (FANETs): A survey” *Ad Hoc Networks*, vol. 11, no. 3, pp. 1254–1270, May 2013. [Online]. Available: http://dx.doi.org/10.1016/j.adhoc.2012.12.004

[7] O. Sahingoz, “Mobile networking with UAVs: Opportunities and challenges,” in *Proc. ICUAS*, May 2013, pp. 933–941.

[8] K. Zhang, W. Zhang, and J.-Z. Zeng, “Preliminary study of routing and date integrity in mobile Ad Hoc UAV network,” in *Proc. ICACIA*, Dec. 2008, pp. 347–350.

[9] J. Chroboczek, “The Babel routing protocol,” Internet Eng. Task Force (IETF), Fremont, CA, USA, RFC 6126, Apr. 2011. [Online]. Available: http://www.rfc-editor.org/rfc/rfc6126.txt

[10] T. Clausen and P. Jacquet, “Optimized link state routing protocol (OLSR),” Internet Eng. Task Force (IETF), Fremont, CA, USA, RFC 3626, Oct. 2003. [Online]. Available: http://www.rfc-editor.org/rfc/rfc3626.txt

[11] C. Dearlove, T. Clausen, and P. Jacquet, “The optimized link state routing protocol version 2,” Internet Eng. Task Force (IETF), Fremont, CA, USA, Draft RFC draft-ietf-manet-olsrv2-10, 2009. [Online]. Available: http://tools.ietf.org/id/draft-ietf-manet-olsrv2-19.txt

[12] E. W. Frew and T. X. Brown, “Networking issues for small unmanned aircraft systems,” *J. Intell. Robot. Syst.*, vol. 54, no. 1–3, pp. 21–37, Mar. 2009. [Online]. Available: http://dx.doi.org/10.1007/s10846-008-9253-2

[13] Y. Guo, X. Li, H. Yousefi’zadeh, and H. Jafarkhani, “UAV-aided cross-layer routing for MANETs,” in *Proc. IEEE WCNC*, Apr. 2012, pp. 2928–2933.

[14] A. Alshbatat and L. Dong, “Cross layer design for mobile Ad-Hoc unmanned aerial vehicle communication networks,” in *Proc. ICNSC*, Apr. 2010, pp. 331–336.

[15] M. Benzaid, P. Minet, and K. Al Agha, “Integrating fast mobility in the OLSR routing protocol,” in *Proc. 4th Int. Workshop Mobile Wireless Commun. Netw.*, 2002, pp. 217–221.

[16] M. Benzaid, P. Minet, and K. Al-Agha, “Analysis and simulation of fast-OLSR,” in *Proc. 57th IEEE Semiannu. VTC—Spring*, Apr. 2003, vol. 3, pp. 1788–1792.

[17] S. Rosati, K. Krużelecki, L. Traynard, and B. Rimoldi, “Speed-aware routing for UAV Ad-Hoc networks,” in *Proc. 4th Int. IEEE Workshop Wireless Netw. & Control Unmanned Auton. Veh.: Archit., Protocols Appl.*, 2013, pp. 1788–1792.

[18] Sensefly eBee. [Online]. Available: http://www.sensefly.com/drones/ebee.html

[19] SMAVNET II website. [Online]. Available: http://smavnet.epfl.ch

[20] olsrd Link Quality Extensions. [Online]. Available: http://www.olsr.org/docs/README-Link-Quality.html

[21] D. S. J. De Couto, D. Aguayo, J. Bicket, and R. Morris, “A high-throughput path metric for multi-hop wireless routing,” in *Proc. 9th Annu. Int. Conf. MobiCom*, New York, NY, USA, 2003, pp. 134–146. [Online]. Available: http://doi.acm.org/10.1145/938985.939000

[22] Optimized Link State Routing Deamon. [Online]. Available: http://www.olsr.org/

[23] Microhard Systems Inc. Spread Spectrum Wireless Modem. [Online]. Available: http://www.microhardcorp.com/n2420.php

[24] Gumstix Web Page: Overo Tide COM Product overview. [Online]. Available: https://www.gumstix.com/store/app.php/products/257/

[25] Extendable Mobile Ad-hoc Network Emulator (EMANE). [Online]. Available: http://cs.itd.nrl.navy.mil/work/emane/

[26] IEEE P802.11 Wireless LANs, “*TGn Channel Models*, ” IEEE Std. 802.11 11-03/940r4, Tech. Rep., 2004.

[27] E. Akim and D. Tuchin, “GPS errors statistical analysis for ground receiver measurements,” Keldysh Inst. Appl. Math., Russia Academy Sci., Moscow, Russia, 2002.

Stefano Rosati (S’07–M’11) received the Laurea degree (summa cum laude) and the Ph.D. degree in telecommunications engineering from the University of Bologna, Bologna, Italy, in 2007 and 2011, respectively.

He is a Postdoctoral Research Engineer with the École Polytechnique Fédérale de Lausanne (EPFL), Lausanne, Switzerland. From 2007 to 2011, he was with the Advanced Research Center for Electronic Systems, University of Bologna. In 2010, he was an Intern Engineer with the Corporate R&D Department, Qualcomm Inc., San Diego, CA, USA. In 2011, he joined the Information Processing Group and the Mobile Communications Laboratory of the EPFL. He has authored several scientific papers and holds international patents regarding his topics of interest. His interests are in various aspects of digital communications, particularly next-generation cellular communication systems, and both terrestrial and satellite broadcast networks. His research activities are also focused on flying ad hoc networks and self-organizing networks of unmanned aerial vehicles.

Karol Krużelecki (M’09) received the M.Sc.Eng. degree in computer science and in computational mechanics from Cracow University of Technology, Cracow, Poland, in September and November 2008, respectively.

He is a Research Engineer with the École Polytechnique Fédérale de Lausanne (EPFL), Lausanne, Switzerland. Between 2008 and 2011, he was with The European Organization for Nuclear Research (CERN) on the development of automatic build and test systems used to improve software quality and reliability for the Large Hadron Collider beauty experiment (LHCb). In 2012, he joined the Information Processing Group and the Mobile Communications Laboratory of the EPFL.

Grégoire Heitz received the M.Sc. degree in electronics from the ENSCPE, Lyon, France, in 2012.

He was with SenseFly SA for his master thesis, working on the development of a new flying robot in 2011. Since September 2012, he has been an Engineer with the Laboratory of Intelligent System, École Polytechnique Fédérale de Lausanne, Lausanne, Switzerland. His research interest lies in embedded systems development.

Dario Floreano (SM’06) received the M.A. degree from the University of Trieste, Trieste, Italy, in 1988; the M.S. degree from the University of Stirling, Stirling, U.K., in 1991; and the Ph.D. degree from the University of Trieste in 1995.

He is a Full Professor with the École Polytechnique Fédérale de Lausanne, Lausanne, Switzerland, where he is the Director of the Laboratory of Intelligent Systems and of the Swiss National Center of Competence in Robotics. He has authored more than 300 peer-reviewed articles and three books on the topics of evolutionary robotics, bioinspired artificial intelligence, and biomimetic flying robots and has two spin-off companies. His research interests are the convergence of biology, artificial intelligence, and robotics.

Bixio Rimoldi (S’83–M’85–SM’92–F’00) received the Diploma and Doctorate degrees from the Department of Electrical Engineering, Eidgenoössische Technische Hochschule, Zurich, Switzerland.

During 1988–1989, he held visiting positions with the University of Notre Dame, Notre Dame, IN, USA; and Stanford University, Stanford, CA, USA. In 1989, he joined the Faculty of Electrical Engineering, Washington University, St. Louis, MO, USA, and since 1997, he has been a Full Professor with the École Polytechnique Fédérale de Lausanne (EPFL), Lausanne, Switzerland, as well as the Director of the Mobile Communications Laboratory. He has spent sabbatical leaves with the Massachusetts Institute of Technology, Cambridge, MA, USA, (2006) and at the University of California, Berkeley, CA (2003–2004). His interests are in various aspects of digital communications, particularly information theory and software-defined radio.

Dr. Rimoldi received the US National Science Foundation Young Investigator Award in 1993. During 2002–2009, he was on the Board of Governors of the IEEE Information Theory Society, where he served in several offices including President. He was a Cochairman, with B. Hajek, of the 1995 IEEE Information Theory Workshop on Information Theory, Multiple Access, and Queueing (St. Louis), and a Cochairman, with J. Massey, of the 2002 IEEE International Symposium in Information Theory (Lausanne). He was a member of the Editorial Board of “Foundations and Trends on Communications and Information Theory” and was an Editor of the *European Transactions on Telecommunications*. During 2005–2006, he was the Director of EPFL’s undergraduate program in communication systems.